Kcne3 deletion initiates extracardiac arrhythmogenesis in mice

Zhaoyang Hu,[*,†,‡] Shawn M. Crump,[*,†,‡] Marie Anand,[*,†,‡] Ritu Kant,[*,†,‡] Roberto Levi,[§] and Geoffrey W. Abbott[*,†,‡,1]

[*]Bioelectricity Laboratory, [†]Department of Pharmacology, and [‡]Department of Physiology and Biophysics, School of Medicine, University of California, Irvine, California, USA; and [§]Department of Pharmacology, Weill Cornell Medical College, New York, New York, USA

ABSTRACT **Mutations in the human *KCNE3* potassium channel ancillary subunit gene are associated with life-threatening ventricular arrhythmias. Most genes underlying inherited cardiac arrhythmias, including *KCNE3*, are not exclusively expressed in the heart, suggesting potentially complex disease etiologies. Here we investigated mechanisms of *KCNE3*-linked arrhythmogenesis in *Kcne3*$^{-/-}$ mice using real-time qPCR, echo- and electrocardiography, ventricular myocyte patch-clamp, coronary artery ligation/reperfusion, blood analysis, cardiac synaptosome exocytosis, microarray and pathway analysis, and multitissue histology. *Kcne3* transcript was undetectable in adult mouse atria, ventricles, and adrenal glands, but *Kcne3*$^{-/-}$ mice exhibited 2.3-fold elevated serum aldosterone ($P=0.003$) and differentially expressed gene networks consistent with an adrenal-targeted autoimmune response. Furthermore, 8/8 *Kcne3*$^{-/-}$ mice *vs.* 0/8 Kcne3$^{+/+}$ mice exhibited an activated-lymphocyte adrenal infiltration ($P=0.0002$). *Kcne3* deletion also caused aldosterone-dependent ventricular repolarization delay (19.6% mean QT_c prolongation in females; $P<0.05$) and aldosterone-dependent predisposition to postischemia arrhythmogenesis. Thus, 5/11 *Kcne3*$^{-/-}$ mice *vs.* 0/10 Kcne3$^{+/+}$ mice exhibited sustained ventricular tachycardia during reperfusion ($P<0.05$). *Kcne3* deletion is therefore arrhythmogenic by a novel mechanism in which secondary hyperaldosteronism, associated with an adrenal-specific lymphocyte infiltration, impairs ventricular repolarization. The findings highlight the importance of considering extracardiac pathogenesis when investigating arrhythmogenic mechanisms, even in inherited, monogenic channelopathies.—Hu, Z., Crump, S. M., Anand, M., Kant, R., Levi, R., Abbott, G. W. *Kcne3* deletion initiates extracardiac arrhythmogenesis in mice. *FASEB J.* 28, 935–945 (2014). www.fasebj.org**

Key Words: long-QT syndrome · β *subunit* · *potassium channel*

SUDDEN CARDIAC DEATH (SCD) is a leading global cause of mortality and accounts for the annual loss of >300,000 adult lives in the United States alone. Potential causes of SCD are multifactorial, but in most cases, the underlying cause is thought to be a lethal ventricular tachyarrhythmia developed in the context of existing ischemic cardiac disease. However, up to 30% of SCD victims die without any obvious structural heart defects at autopsy (1). These cases, most notably in younger individuals, are thought to predominantly occur because of inherited channelopathies. Mutations in genes encoding ion channel proteins (most commonly, but not exclusively, voltage-gated sodium or potassium channels) and the proteins that regulate them are responsible for life-threatening cardiac arrhythmias that predispose to SCD. These arrhythmias include long-QT syndrome (LQTS), short-QT syndrome, Brugada syndrome (BrS), and catecholaminergic polymorphic ventricular tachycardia (VT) (2).

The potential mechanisms underlying SCD, or even the arrhythmia syndromes that underlie many cases of SCD, have not been completely clarified. The majority of mutations linked to ventricular arrhythmias are within the genes encoding the KCNQ1 (Kv7.1) and KCNH2 (hERG) voltage-gated potassium (K_V) channel pore-forming or α subunits (2). The mechanistic basis for these arrhythmias is, logically, considered to stem from disruption of the ventricular myocyte K^+ currents that these channels conduct.

Mutations in the genes encoding ancillary (β) subunits that coassemble with K_V α-subunits to modulate their trafficking and functional attributes also contribute to arrhythmogenesis. Thus, these β subunits are essential for normal cardiac rhythm (3). Interestingly, the majority of ion channel pore-forming subunits and regulatory subunits linked to cardiac arrhythmias are also expressed in tissues outside the heart. This suggests that monogenic arrhythmogenic channelopathies may be complex syndromes involving more than direct disruption of ventricular ion currents.

Abbreviations: 4-AP, 4-aminopyridine; AUC, area under the curve; BrS, Brugada syndrome; DEG, differentially expressed gene; ECG, electrocardiogram; H&E, hematoxylin and eosin; K_V, voltage-gated potassium; LAD, left anterior descending coronary artery; LQTS, long-QT syndrome; NE, norepinephrine; SCD, sudden cardiac death; TEA, tetraethylammonium; VT, ventricular tachycardia

[1] Correspondence: 360 Medical Surge II, Department of Pharmacology, School of Medicine, University of California, Irvine, CA 92697, USA. E-mail: abbottg@uci.edu

doi: 10.1096/fj.13-241828

This article includes supplemental data. Please visit *http://www.fasebj.org* to obtain this information.

Here, studying a gene-targeted mouse, we investigated the potential for ventricular arrhythmogenesis arising from disruption of the *Kcne3* gene. *Kcne3* encodes a single transmembrane domain K_V channel ancillary subunit (Kcne3) that associates with and regulates a range of K_V channel α subunits (3). Despite an absence of detectable expression in adult mouse heart, *Kcne3* deletion delayed ventricular repolarization and increased the frequency and duration of ventricular arrhythmogenesis during reperfusion immediately following transient ischemia. We present evidence supporting a novel arrhythmogenic mechanism of extracardiac origin that may also contribute to human *KCNE3*-linked ventricular arrhythmias, which include LQTS and BrS.

MATERIALS AND METHODS

Transgenic mouse generation, care, and use

We created a global *Kcne3*$^{-/-}$ mouse line by homologous recombination as described previously (4) and then analyzed *Kcne3* tissue expression and the effects of *Kcne3* disruption by comparing *Kcne3*$^{-/-}$ mice to age-matched *Kcne3*$^{+/+}$ littermates. The study was approved by the Animal Care and Use Committees at Weill Cornell Medical College and University of California–Irvine, and was carried out in strict accordance with the recommendations in the Guide for the Care and Use of Laboratory Animals of the U.S. National Institutes of Health. For baseline electrocardiography, because we have previously observed age-dependent QT interval lengthening in wild-type mice, 2 age groups of adult mice were used, 5 and 9 mo old. For cellular electrophysiology and ischemia-reperfusion arrhythmia experiments, only 9-mo-old mice were studied. Mean ages at time of experiment in the 5-mo-old group were *Kcne3*$^{+/+}$, 5.3 ± 0.2 mo, $n = 16$; *Kcne3*$^{-/-}$, 5.2 ± 0.3 mo, $n = 12$. Mean ages at time of experiment in the 9-mo-old group were *Kcne3*$^{+/+}$, 9.3 ± 0.2 mo, $n = 46$; *Kcne3*$^{-/-}$, 8.5 ± 0.2 mo, $n = 47$. Both female and male mice were studied for most experiments, and data pooled only if no sex-dependent differences were observed, and only when pooling was needed to generate a large enough *n*. Where indicated, spironolactone (Sigma-Aldrich, St. Louis, MO, USA), an aldosterone receptor competitive antagonist, was administered by intraperitoneal injection (50 mg/kg) once daily for 7 d before functional assays. Mean ages of mice used for other assays are indicated where appropriate.

Electrocardiography and hemodynamic study

Mice were anesthetized with isoflurane (2%) and placed in a supine position. Surgical anesthesia was verified as a lack of response to toe pinch. The standard limb lead II configuration electrocardiographic system was attached to the limb subcutaneously by needle electrodes, and electrocardiograms (ECGs) were recorded throughout the study. QT, RR, PR, and QRS intervals and heart rate were quantified. QT_c was calculated based on a variant of Bazett's formula modified specifically for mice (5). For hemodynamic analysis, the right carotid artery was exposed through a cervical midline incision, and the left ventricle was catheterized *via* the right carotid artery using a 1.0 F Millar Micro-Tip catheter transducer (model SPR-1000) connected to a pressure transducer (Millar Instruments, Houston, TX, USA). Baseline blood pressures were recorded before advancing the catheter into the left ventricle. The real-time data were collected with a Powerlab/8sp system (AD Instruments, Colorado Springs, CO, USA). LabChart 7.2.1 software (AD Instruments) was used for ECG and hemodynamic data acquisition and analysis.

Coronary artery ligation and reperfusion

Mice were anesthetized with isoflurane (2%) and placed in a supine position under a stereomicroscope. The neck and chest regions were shaved and cleaned with ethanol. Mechanical ventilation was achieved by orotracheal intubation with an endotracheal tube (PE90) attached to a mouse ventilator (Harvard Apparatus, Holliston, MA, USA) and ventilated with a mixture of 2% isoflurane and 98% oxygen. The respiratory rate was maintained at 150 strokes/min with a tidal volume of 250 μl. After a left thoracotomy, the left anterior descending coronary artery (LAD) was located. A 9-0 polyamide suture (Ethilon) was passed underneath the LAD close to its origin, for coronary artery occlusion and reperfusion. Myocardial ischemia was confirmed by ST segment elevation in ECG, epicardial cyanosis, and restricted ventricular motion. All mice were subjected to 10 min of ischemia followed by 20 min reperfusion, the latter confirmed by epicardial hyperemia. ECGs were recorded using with a BioAmp connected to a PowerLab system (AD Instruments). A heating pad was used to prevent hypothermia throughout the experiments. For ligation studies, we used the following mice: untreated, 7 male and 3 female wild-type mice, 8 male and 3 female *Kcne3*$^{-/-}$ mice; spironolactone-treated, 5 male and 4 female wild-type mice, 4 male and 6 female *Kcne3*$^{-/-}$ mice. We did not observe sex dependence to the outcomes, and so we pooled data from both sexes.

Histology and immunofluorescence

For histology, mice were euthanized and perfused through the left ventricle with PBS; hearts and adrenal glands were then taken and fixed in 4% paraformaldehyde in PBS overnight at room temperature. Following fixation in formaldehyde, dehydration, and embedding in paraffin, consecutive 5-μm sections of hearts including the left ventricular walls and the septums were cut with a microtome. Heart architecture was determined by staining with hematoxylin and eosin (H&E); fibrosis was probed by Masson's Trichrome stain. For adrenal immunofluorescence analysis, frozen adrenal sections were fixed in ice-cold acetone and incubated with 1:1000 phycoerythrin fluorophore-conjugated hamster anti-mouse CD30 in 10% BSA blocking buffer after 1 h blocking in the absence of antibody, with 3 × 5-minute pre- and post-washes for every step using PBS. Sections were then mounted with DAPI-labeling mounting medium and visualized 1 d later using an Olympus BX51 microscope and CellSens software (Olympus, Center Valley, PA, USA).

Blood analysis

Blood was collected in heparin-treated capillary tubes followed by centrifugation (4000 rpm, 10 min). Serum was obtained and stored at −20°C before use. Serum aldosterone was determined using ELISA (Cayman Chemical Company, Ann Arbor, MI, USA). Serum angiotensin II was quantified using ELISA (Abnova, Walnut, CA, USA). Serum cholesterol was quantified using a cholesterol oxidase color reaction kit (Abcam, Cambridge, MA, USA). For blood glucose measurements, blood was taken from the tail tip and glucose measured using a OneTouch Ultra blood glucose meter (LifeScan, Milpitas, CA, USA). For fasting intraperitoneal glucose

tolerance testing, after 6 h of food withdrawal, glucose (2 g/kg body weight) was injected intraperitoneally, and a drop of blood was collected from the tail tip at 0, 15, 30, 60, and 120 min for glucose quantification. The corresponding relative area under the curve (AUC) for glucose concentration was calculated using the trapezoid rule. Serum and blood parameters were determined by investigators blinded to the mouse genotype.

Real-time qPCR

Mice were euthanized by CO_2 asphyxiation followed by cervical dislocation. Adrenal glands, hearts, and stomachs were harvested, washed in PBS, then processed or stored at −80°C until use. RNA was extracted using 1 ml of Trizol (Invitrogen, Carlsbad, CA, USA) per 100 mg of tissue and purified using the RNeasy Mini Kit (Qiagen, Hilden, Germany) according to the manufacturer's protocol. RNA samples with A_{260}/A_{280} absorbance ratios between 2.00 and 2.20 were used for further synthesis. RNA (500 ng to 1 μg) was used for cDNA synthesis (Qiagen's Quantitect Reverse Transcriptase) and stored at −20°C until use. Primer pairs for target genes *Kcne3* [U.S. National Center for Biotechnology Information (NCBI; Bethesda, MD, USA) GeneID 57442] and *Gapdh* (NCBI GeneID 14433) produced amplicons of 143 and 123 bp, respectively. Sequences of qPCR primers (0.05-μm scale, HPLC purified; Sigma-Aldrich) were as in the Harvard Medical School Primer Bank (Boston, MA, USA), as follows: *Kcne3*, 5′-ATGGAGACTTCCAACGGGACT-3′, and reverse 5′-GCCCGACGATCCTCAGTTTG-3′; and *Gapdh,* forward 5′-AGGTCGGTGTGAACGGATTTG-3′, and reverse 5′-TGTAGACCATGTAGTTGAGGTCA-3′. Real-time qPCR analysis was performed using the CFX Connect System, iTaq Universal SYBR Green Supermix (Bio-Rad, Hercules, CA, USA) and 96-well clear plates. Thermocycling parameters were set according to the manufacturer's protocol for iTaq. Samples were run in triplicate as a quality control measure, and triplicates with an SD ≥ 0.500 were repeated. Melting curves were assessed for verification of a single product. Relative expression levels were compared by calculating $\Delta\Delta C_q$ values.

Whole-transcript microarray analysis

Mice were euthanized, and tissue and blood were harvested and preserved in RNA*later* (Invitrogen) until use. Total RNA was collected from adrenal glands and blood, reverse-transcribed into cDNA, and analyzed by whole-transcript transcriptomics using the GeneAtlas microarray system (Affymetrix, Santa Clara, CA, USA) and the manufacturer's protocols. MoGene 1.1 ST array strips (Affymetrix) were used to hybridize to newly synthesized sscDNA. Each array comprised 770,000 probes to probe ~28,000 genes, with a median 28 probes/transcript. Statistical analysis was performed using Partek Express software (Partek, St. Louis, MO, USA) and the Affymetrix Mouse Gene 1.1 ST Array Plate and Strip Analysis library file. Gene expression changes associated with *Kcne3* deletion were analyzed using the Ingenuity Systems iReport (Ingenuity Systems, Inc., Redwood, CA, USA; http://www.ingenuity.com) to identify biological processes, pathways, and diseases associated with the identified differentially expressed genes (DEGs). Expression changes of ≥1.5-fold and $P < 0.05$ after false discovery rate correction were considered significant by Ingenuity's knowledge base and included in the analysis.

Isolation of adult mouse ventricular myocytes

Adult (9-mo-old) *Kcne3*$^{+/+}$ and *Kcne3*$^{-/-}$ mice were euthanized, and their hearts were rapidly excised and mounted by aortic cannulation onto a Langendorff apparatus (Harvard Apparatus). Then, hearts were perfused with warmed (37°C), oxygenated, calcium-free HEPES buffer containing (in mM) 137 NaCl, 5.4 KCl, 1.2 $MgSO_4$, 15 NaH_2PO_4, 10 glucose, 10 HEPES, and 2 L-glutamine (pH 7.3; buffer A). After 5 min, 0.36 mg/ml type II collagenase (Worthington, Lakewood, NJ, USA) and 10 μM $CaCl_2$ (buffer B) were added to the solution, and hearts were perfused for 10–14 min, with the temperature maintained at 37°C. Following the perfusion, the atria and free right ventricular wall were removed using a fine scalpel. The left ventricle was cut open, and the ventricular septum and the upper 0.3 mm of tissue at the apex of the left ventricle were removed. These tissue pieces were transferred to a Falcon tube containing prewarmed buffer A supplemented with 5 mg/ml BSA and 150 μM $CaCl_2$ (buffer C). After mechanical dispersion by gentle shaking at 37°C, cells were collected by sedimentation. Isolated myocytes were maintained in buffer A supplemented with 5 mg/ml BSA, and 1 mM $CaCl_2$ solution. Rod-shaped, striated myocytes of healthy appearance with no spontaneous contractions were subjected to electrophysiological recording within the first 24 h following isolation.

Cellular electrophysiology

Whole-cell patch-clamp recordings from adult cardiomyocytes were performed at room temperature using an IX50 inverted microscope (Olympus) equipped with an FHD chamber (IonOptix, Milton, MA, USA), a Multiclamp 700A Amplifier, a Digidata 1300 Analog/Digital converter and PC with pClamp9 software (Molecular Devices, Sunnyvale, CA, USA). Bath solution was (in mM) 117 NaCl, 4 KCl, 1.7 $MgCl_2$, 10 HEPES, 1 KH_2PO_4, 4 $NaHCO_3$, 3 $CoCl_2$, and 10 D-glucose (pH 7.4 with NaOH). Pipettes were of 2.5- to 4-MΩ resistance when filled with intracellular solution containing (in mM) 130 KCl, 2 $MgCl_2$, 20 HEPES, 11 EGTA, 5 Na_2ATP, 0.4 Na_2GTP, and 5 Na_2CTP (pH 7.4 with KOH). Cells were stepped from a holding potential of −70 mV to test potentials from −60 to +60 mV in 20-mV increments. Current amplitudes were normalized to whole-cell membrane capacitance. Data were analyzed using pClamp9.1 software (Molecular Devices), and statistical analysis (ANOVA) was performed using Origin 6.1 software (Microcal, Northampton, MA, USA).

Outward K^+ currents were evoked during 4.5-s voltage steps to test potentials between −60 and + 60 mV in 20-mV increments from a holding potential of −70 mV after a 100 ms prepulse to −40 mV. Leak currents were always <100 pA and were not corrected for. For inhibition of K^+ currents with 4-aminopyridine (4-AP; ICN Biomedicals, Irvine, CA, USA) and tetraethylammonium (TEA; Sigma-Aldrich), stock solutions were prepared in bath solution, applied directly to the bath after baseline recordings, and allowed to equilibrate for 2–3 min before drug recordings. The tau of I_{Kslow} was determined by fitting the decay phases of the K^+ outward currents to the sum of 3 exponentials, as described previously (6). When necessary for fitting, C was fixed to the steady-state current value at the end of the test pulse. Correlation coefficients were determined to assess the quality of fits; only fits with correlation coefficients > 0.970 were used in this study.

Echocardiography

Transthoracic echocardiograms were recorded in 2-mo-old conscious-sedated (1% isoflurane in 100% oxygen) *Kcne3*$^{+/+}$ and *Kcne3*$^{-/-}$ mice using a Sequoia C256 and 15L8 probe (Acuson, Mountain View, CA, USA). Left ventricular internal

dimension, posterior wall thickness, internal dimension, posterior and anterior wall thickness, and volume were measured in both diastole and systole, as was intraventricular septum width, at the level of the papillary muscles on the short-axis view using 2-dimensional guided M-mode imaging at 3 cardiac cycles. Left ventricular (LV) fractional shortening (FS) was calculated from the M-mode recordings using the equation FS (%) = (LV end-diastolic dimension − LV end systolic dimension)/(LV end-diastolic dimension) × 100.

Norepinephrine (NE) release from mouse cardiac synaptosomes

Seven male *Kcne3*$^{+/+}$ and 7 male *Kcne3*$^{-/-}$ mice were euthanized by cervical dislocation under light anesthesia with CO_2 vapor in accordance with institutional guidelines. The ribcage was dissected away, and the heart was rapidly excised, freed from fat and connective tissue, and transferred to a Langendorff apparatus (Radnoti Glass Technology, Monrovia, CA, USA). The aorta was cannulated with a flanged 18-gauge stainless-steel needle. Spontaneously beating hearts were perfused through the aorta in a retrograde mode at a constant pressure of 100 cm of H_2O with modified Krebs-Henseleit buffer containing (mM) 120 NaCl, 4.7 KCl, 2.5 $CaCl_2$, 1.2 $MgSO_2$, 1.2 KH_2PO_4, 25 $NaHCO_3$, 11 glucose, and 0.5 EDTA. The perfusion fluid was equilibrated with 95% O_2 + 5% CO_2 at 37°C to give a pH of 7.4. Spontaneously beating hearts were perfused through the aorta for 15 min; this procedure ensured that no blood traces remained in the coronary circulation. At the end of the 15 min perfusion, hearts were minced in ice-cold 0.32 M sucrose containing 1 mM EGTA (pH 7.4). Minced tissue was digested with 40 mg collagenase (type II; Worthington) per 10 ml of 0.32 M sucrose solution per gram of wet heart weight for 1 h at 37°C. The sucrose solution contained 1 mM pargyline to prevent enzymatic destruction of synaptosomal NE. After low-speed centrifugation (10 min at 120 *g* and 4°C), the resulting pellet was suspended in 10 volumes of 0.32 M sucrose and homogenized with a Teflon/glass homogenizer. The homogenate was spun at 650 *g* for 10 min at 4°C, and the pellet was rehomogenized and respun. The pellet containing cellular debris was discarded, and the supernatants from the last 2 spins were combined and equally divided into 4 tubes. Each tube was centrifuged for 20 min at 20,000 *g* at 4°C. This pellet, which contained cardiac synaptosomes, was resuspended in HEPES-buffered saline to a final volume of 500 μl in a water bath at 37°C. Each suspension functioned as an independent sample and was used only once. In every experiment, one sample was untreated (control, basal NE release), and others were incubated with KCl (3, 10, or 30 mM) for 20 min. At the end of the incubation period, each sample was centrifuged for 20 min (20,000 *g* at 4°C). The supernatant was assayed for NE content by high-pressure liquid chromatography, and the pellet was assayed for protein content by a modified Lowry procedure (7). Although the presence of sympathetic nerve endings in the synaptosomal preparation was not verified by electron microscopy, murine cardiac synaptosomes responded to K^+ depolarization with a concentration-dependent NE release (see Results). Values were expressed as mean ± SEM percentage increases above basal NE release.

Statistical analyses

All values are expressed as means ± SE. Unless described otherwise, statistical comparisons between 2 groups of values were performed using 2-tailed Student's *t* tests. For multiple comparisons, ANOVA was used to evaluate the statistical difference among different groups followed by the Bonferroni test. Fisher's exact test was used to compare numbers of mice falling into one of 2 groups, *e.g.*, sinus rhythm *vs.* arrhythmia, except for the sustained VT comparison, for which χ^2 was used. For either test type, significance was assumed for values of $P < 0.05$.

RESULTS

Age- and sex-dependent effects of *Kcne3* deletion on ventricular repolarization

While older (9-mo-old) mice of either genotype exhibited longer QT and QT_c intervals than younger (5-mo-old) mice regardless of genotype, *Kcne3* deletion also caused a general trend toward delayed repolarization. This genotype-dependent effect achieved statistical significance ($P<0.05$) only between mice of similar age when comparing 9-mo-old female *Kcne3*$^{-/-}$ *vs.* *Kcne3*$^{+/+}$ mice. However, there was an age- and *Kcne3*-dependent QTc prolongation in the male *Kcne3*$^{-/-}$ mice (9-mo-old *Kcne3*$^{-/-}$ *vs.* 5-mo-old *Kcne3*$^{+/+}$). Other ECG parameters, including RR, PR, and QRS intervals, were unaffected by genotype (**Fig. 1**). *Kcne3* deletion had no detectable effects on cardiac architecture as assessed by echocardiography, normalized heart mass, and histology (Supplemental Fig. S1*A–C*).

Whole-cell patch-clamp recordings (**Fig. 2**) from ventricular myocytes acutely isolated from 9-mo-old mice revealed that *Kcne3* deletion had no statistically significant effects on steady-state or peak current density (Fig. 2*A, C*), although septal (but not apex) myocytes from female *Kcne3*$^{-/-}$ mice exhibited slower mean $I_{K,slow}$ inactivation (Fig. 2*B–D*). In adult mouse ventricular myocytes, $I_{K,slow}$ is generated primarily by Kv1.5 ($I_{K,slow1}$) and Kv2.1 ($I_{K,slow2}$), inhibited by 50 μM 4-AP and 1 mM TEA, respectively (6). No significant shift in current density of either component was revealed using these pharmacological tools (Fig. 2*E, F*), supporting the hypothesis that *Kcne3* deletion slowed the inactivation of one or both of these channel types rather than altering the balance of their respective current density. Neither of the rapid current decay components, reflecting $I_{to,f}$ and $I_{to,s}$ inactivation, showed altered kinetics in either apex or septa of female *Kcne3*$^{-/-}$ mice. Septal myocytes from male mice showed no statistically significant, genotype-dependent differences in current density or kinetics, although there was a trend toward slower $I_{K,slow}$ inactivation in myocytes from male *Kcne3*$^{-/-}$ mice (Fig. 2*G, H*) as was observed in septal myocytes from female mice.

Kcne3 transcript is not detectable in adult mouse heart

KCNE subunits directly modulate K_V channels, and it is generally assumed that KCNE-linked arrhythmogenesis arises primarily from direct disruption of KCNE-containing cardiac K_V channel complexes (8). Here *Kcne3* transcript levels in left and right atria and ventricles isolated from adult *Kcne3*$^{+/+}$ mice were indistinguish-

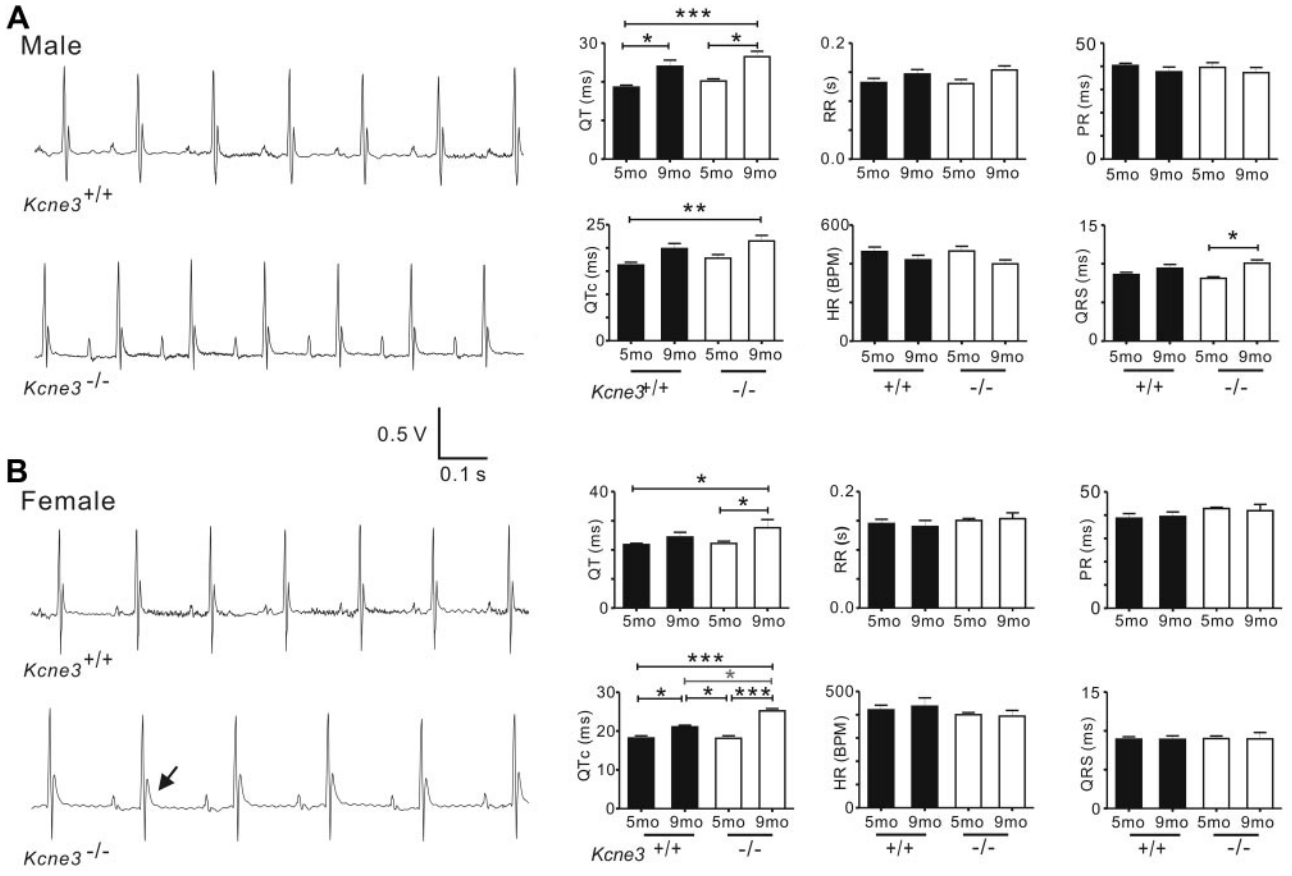

Figure 1. Kcne3 deletion age-dependently delays ventricular repolarization. *A*) Left panel: representative surface ECGs of male 9-mo-old $Kcne3^{+/+}$ and $Kcne3^{-/-}$ mice. Right panel: mean ECG parameters of male $Kcne3^{+/+}$ (5 mo old, n=8; 9 mo old, n=10) and $Kcne3^{-/-}$ mice (5 mo old, n=5; 9 mo old, n=11). $^{*}P < 0.05$, $^{**}P < 0.01$, $^{***}P < 0.001$ *vs.* $Kcne3^{+/+}$. *B*) Left panel: representative ECGs of female 9-mo-old $Kcne3^{+/+}$ and $Kcne3^{-/-}$ mice. Arrow: prolonged T wave. Right panel: mean ECG parameters of female $Kcne3^{+/+}$ (5 mo old, n=8; 9 mo old, n=4) and $Kcne3^{-/-}$ mice (5 mo old o, n=7; 9 mo old, n=3). $^{*}P < 0.05$, $^{***}P < 0.001$ *vs.* $Kcne3^{+/+}$.

able from levels in the same tissues isolated from adult $Kcne3^{-/-}$ mice, indicating negligible cardiac *Kcne3* expression. In contrast, *Kcne3* was readily detectable in adult $Kcne3^{+/+}$ mouse colon but not adult $Kcne3^{-/-}$ mouse colon (**Fig. 3*A***). These findings were similar in both female and male mice and are consistent with a previous report of an independently generated $Kcne3^{-/-}$ mouse line of a different strain (9).

Kcne3 deletion causes hyperaldosteronism and hypercholesterolemia

As KCNE3 is expressed in tissues other than the heart, including various epithelia, we examined other potential causes for predisposition to arrhythmias in $Kcne3^{-/-}$ mice. The renin-angiotensin-aldosterone system plays an important role in regulating blood pressure, ion, and fluid homeostasis and influences arrhythmogenesis. Here we found that *Kcne3* deletion in mice alters neither blood pressure, left ventricular pressure (Supplemental Fig. S1*D–G*), nor serum angiotensin II concentration (Fig. 3*B*). In contrast, the serum aldosterone concentration of $Kcne3^{-/-}$ mice was 2.3-fold higher than that of $Kcne3^{+/+}$ mice (n=9, P=0.003; Fig. 3*B*). Furthermore, *Kcne3* deletion led to hypercholesterolemia, increasing free and total serum LDL, while reducing free serum HDL (Fig. 3*C*).

Kcne3 deletion affects neither serum K^+, glucose regulation, nor exocytosis of endogenous norepinephrine from cardiac sympathetic nerve terminals.

Consistent with previous reports (9), *Kcne3* deletion did not alter serum K^+ (Fig. 3*D*), suggesting against serum K^+ perturbation being a potential mechanism for chronic stimulation of aldosterone production in $Kcne3^{-/-}$ mice. Mice and humans with disrupted KCNQ1 (a partner of KCNE3 in some tissues, *e.g.*, the colon; ref. 9) exhibit glucose dysregulation, but we did not find evidence for glucose dysregulation in $Kcne3^{-/-}$ mice (Fig. 3*E, F*). Local renin-angiotensin system activity in the heart, measured by quantifying NE release from cardiac synaptosomes isolated from $Kcne3^{+/+}$ and $Kcne3^{-/-}$ mice (10), was also unaffected. Thus, depolarization of cardiac synaptosomes from $Kcne3^{+/+}$ mice with 3, 10, and 30 mM K^+ resulted in a concentration-dependent increase of ~7, ~11, and ~22%, respectively, in NE release

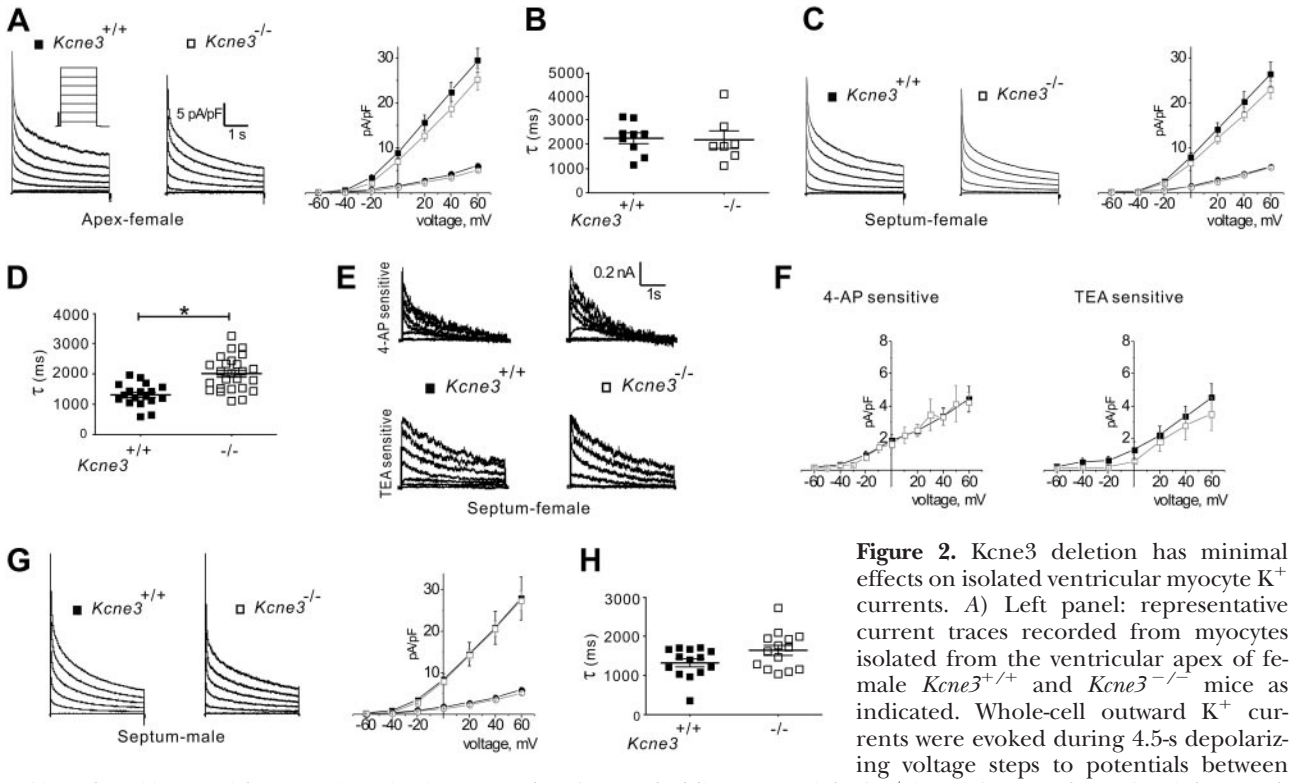

Figure 2. Kcne3 deletion has minimal effects on isolated ventricular myocyte K^+ currents. *A*) Left panel: representative current traces recorded from myocytes isolated from the ventricular apex of female *Kcne3*$^{+/+}$ and *Kcne3*$^{-/-}$ mice as indicated. Whole-cell outward K^+ currents were evoked during 4.5-s depolarizing voltage steps to potentials between −60 and + 60 mV with an I_{Na}-inactivating prepulse, from a holding potential of −70 mV (protocol inset). Right panel: mean *I/V* relation for peak (squares) and end-of-pulse (circles) currents recorded from myocytes as at left; n = 13–15 cells/genotype. *B*) Mean $I_{K,slow}$ inactivation τ at +40 mV for apex myocytes as in *A*, n = 13–15 cells/genotype. *C*) Left panel: representative current traces recorded from $I_{to,f}$-expressing myocytes isolated from the ventricular septum of female *Kcne3*$^{+/+}$ and *Kcne3*$^{-/-}$ mice; other parameters as in *A*. Right panel: mean *I/V* relation for peak (squares) and end-of-pulse currents (circles) recorded from myocytes as at left; n = 24–26 cells/genotype. *D*) Mean $I_{K,slow}$ inactivation τ at +40 mV for septal myocytes as in *C*, n = 24–26 cells/genotype. *$P < 0.01$. *E*) Representative digitally subtracted, 4-AP- and TEA-sensitive current waveforms recorded from septal myocytes isolated from female *Kcne3*$^{+/+}$ and *Kcne3*$^{-/-}$ mice. *F*) Mean *I/V* relationships for drug-sensitive currents as in *E*; n = 4–13 myocytes/genotype. *G*) Left panel: representative current traces recorded from $I_{to,f}$-expressing myocytes isolated from the ventricular septum of male *Kcne3*$^{+/+}$ and *Kcne3*$^{-/-}$ mice; other parameters as in *A*. Right panel: mean *I/V* relation for peak (squares) and end-of-pulse currents (circles) recorded from myocytes as at left; n = 22–23 cells/genotype. *H*) Mean $I_{K,slow}$ inactivation τ at +40 mV for septal myocytes as in *G*; n = 22–23 cells/genotype.

above a basal level of 0.8 ± 0.1 pmol/mg (n=14). Similarly, depolarization of cardiac synaptosomes from *Kcne3*$^{-/-}$ mice with 3, 10, and 30 mM K^+ resulted in a concentration-dependent increase in NE release of ~9, ~15, and ~20%, respectively. No significant difference between the 2 respective concentration-response curves was observed (Fig. 3*G*). This dismisses a role for KCNE3 in NE exocytosis elicited by K^+-induced depolarization specifically at the cardiac sympathetic nerve terminals, although it does not rule out more proximal defects. There is currently no evidence in the literature that KCNE3 might play a role in ganglionic transmission. Whether changes might occur even more proximally, *e.g.*, in central sympathetic centers, is also unknown.

Kcne3 deletion causes activated lymphocyte infiltration of the adrenal glands

In the absence of obvious explanations for elevated aldosterone from the preceding data, we pursued a transcriptomics-based approach to understand the cause of hyperaldosteronism in *Kcne3*$^{-/-}$ mice. Adrenal microarrays (**Fig. 4*A***) revealed up-regulation of transcripts consistent with infiltration of lymphocytes, and in particular B cells, in the *Kcne3*$^{-/-}$ adrenals. These included multiple Igκ transcripts, the B-cell chemoattractant chemokine CXCL13 (11), and interleukin-23 receptor, which is expressed on memory T cells but also other immune cells (12, 13). Manual comparison of all transcripts after applying a filter of >2-fold altered expression (P<0.05) revealed that 14/14 up-regulated transcripts in *Kcne3*$^{-/-}$ adrenals were immune response related (Supplemental Fig. S2). Subsequent independent, automated pathway analysis (using a filter of >1.5-fold change and incorporating false discovery rate correction) corroborated these findings and suggested involvement of a STAT4-mediated signaling network (Fig. 4*B*). This analysis also discovered adrenal transcript expression change patterns consistent with autoimmune diseases, most prominently rheumatoid arthritis (Supplemental Fig. S3*A*). *Kcne3*$^{-/-}$ adrenals also clearly exhibited infiltration of large numbers of immune cells that were, in contrast, rarely observed in individual *Kcne3*$^{+/+}$ adrenals (Fig. 4*C*). Clusters of cells positive for CD30, a surface

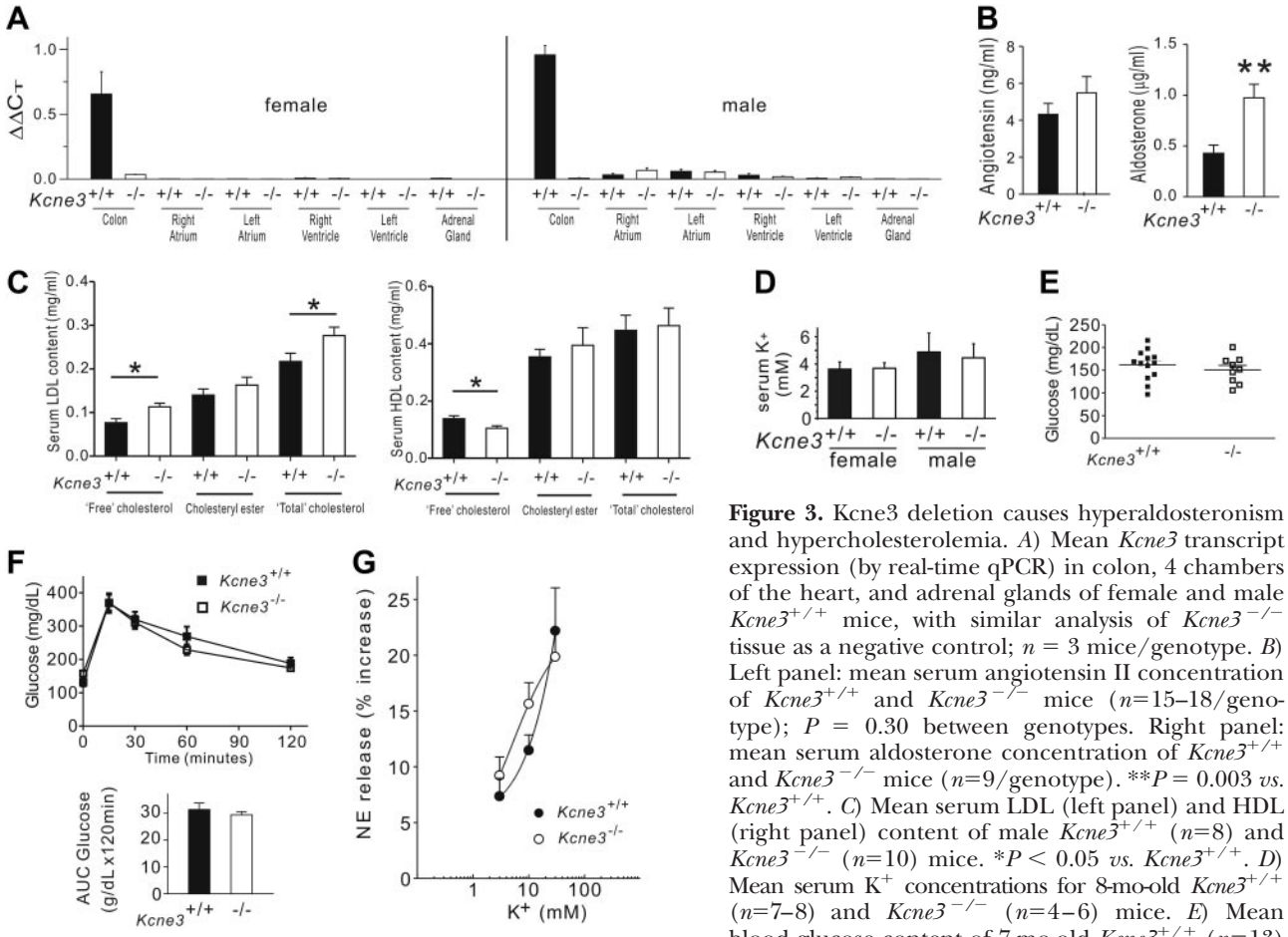

Figure 3. Kcne3 deletion causes hyperaldosteronism and hypercholesterolemia. *A*) Mean *Kcne3* transcript expression (by real-time qPCR) in colon, 4 chambers of the heart, and adrenal glands of female and male $Kcne3^{+/+}$ mice, with similar analysis of $Kcne3^{-/-}$ tissue as a negative control; $n = 3$ mice/genotype. *B*) Left panel: mean serum angiotensin II concentration of $Kcne3^{+/+}$ and $Kcne3^{-/-}$ mice (n=15–18/genotype); $P = 0.30$ between genotypes. Right panel: mean serum aldosterone concentration of $Kcne3^{+/+}$ and $Kcne3^{-/-}$ mice (n=9/genotype). $^{**}P = 0.003$ *vs.* $Kcne3^{+/+}$. *C*) Mean serum LDL (left panel) and HDL (right panel) content of male $Kcne3^{+/+}$ (n=8) and $Kcne3^{-/-}$ (n=10) mice. $^{*}P < 0.05$ *vs.* $Kcne3^{+/+}$. *D*) Mean serum K^+ concentrations for 8-mo-old $Kcne3^{+/+}$ (n=7–8) and $Kcne3^{-/-}$ (n=4–6) mice. *E*) Mean blood glucose content of 7-mo-old $Kcne3^{+/+}$ (n=13) and $Kcne3^{-/-}$ (n=9) mice. *F*) Left panel: mean blood glucose concentrations during glucose tolerance test of 7-mo-old $Kcne3^{+/+}$ (n=13) and $Kcne3^{-/-}$ (n=8) mice. Right panel: area under the curve (AUC) for glucose values from data at left. *G*) Concentration-response curves for the NE-releasing effects of K^+ in synaptosomes isolated from $Kcne3^{+/+}$ and $Kcne3^{-/-}$ mouse hearts. There were no significant differences between the curves. Points are means (n=7 for each point in each curve) of increases in NE release above a basal level of 0.8 ± 0.1 pmol/mg (mean±SE; n=14/genotype).

marker of activated lymphocytes (14), were observed near the medulla/cortex boundary in adrenals of $Kcne3^{-/-}$ but not $Kcne3^{+/+}$ mice (Fig. 4*D*). Finally, microarray analysis of total blood cells again was suggestive of an immune response but was less marked than for the adrenal microarray (Supplemental Fig. S3*B, C*), consistent with an adrenal-targeted response rather than a widespread, systemic infection or systemic autoimmunity. Cardiac, renal, splenic, and skeletal muscle histology revealed no evidence of an inflammatory infiltrate in these other tissues, also consistent with an adrenal-specific infiltration (Supplemental Figs. S1*C* and S3*D–F*).

Kcne3 deletion predisposes to aldosterone-dependent reperfusion arrhythmias

Aldosterone is known to delay ventricular repolarization and increase arrhythmogenesis, including in the context of cardiac ischemia (15, 16). Here we therefore examined the effects on arrhythmogenesis of pretreatment with aldosterone receptor antagonist spironolactone in 9-mo-old $Kcne3^{+/+}$ and $Kcne3^{-/-}$ mice, at baseline and in the context of postischemic reperfusion (following LAD ligation). In contrast to untreated 9-mo-old female $Kcne3^{-/-}$ mice, which showed QTc prolongation compared to 9-mo-old female $Kcne3^{+/+}$ mice (Fig. 1*A*), after 7 d of spironolactone treatment there was no QT_c prolongation in female $Kcne3^{-/-}$ mice (**Fig. 5*A*, *B***). Likewise, spironolactone-pretreated male 9-mo-old mice $Kcne3^{-/-}$ mice exhibited no statistically significant ECG differences compared to pretreated 9-mo-old male $Kcne3^{+/+}$ mice (Fig. 5*A*, *B*; see Supplemental Fig. S4*A*, *B* for sex-pooled data). There was immediate ST-segment elevation after LAD ligation in spironolactone-treated mice, but no statistically significant genotype-dependent differences (Supplemental Fig. S4*C*, *D*). Likewise, normalized heart weights of spironolactone-treated mice were genotype independent (Supplemental Fig. S4*E*).

Strikingly, *Kcne3* deletion increased both the propensity and the duration of ventricular arrhythmogenesis during the immediate postischemic reperfusion period (all recorded arrhythmias began within 30 s of reperfusion; **Fig. 6*A–D***). VT was the class of arrhythmia observed in all but one $Kcne3^{-/-}$ mouse (which exhibited instead atrioventricular block). Representative ECG tracings from $Kcne3^{+/+}$ and $Kcne3^{-/-}$ mice illus-

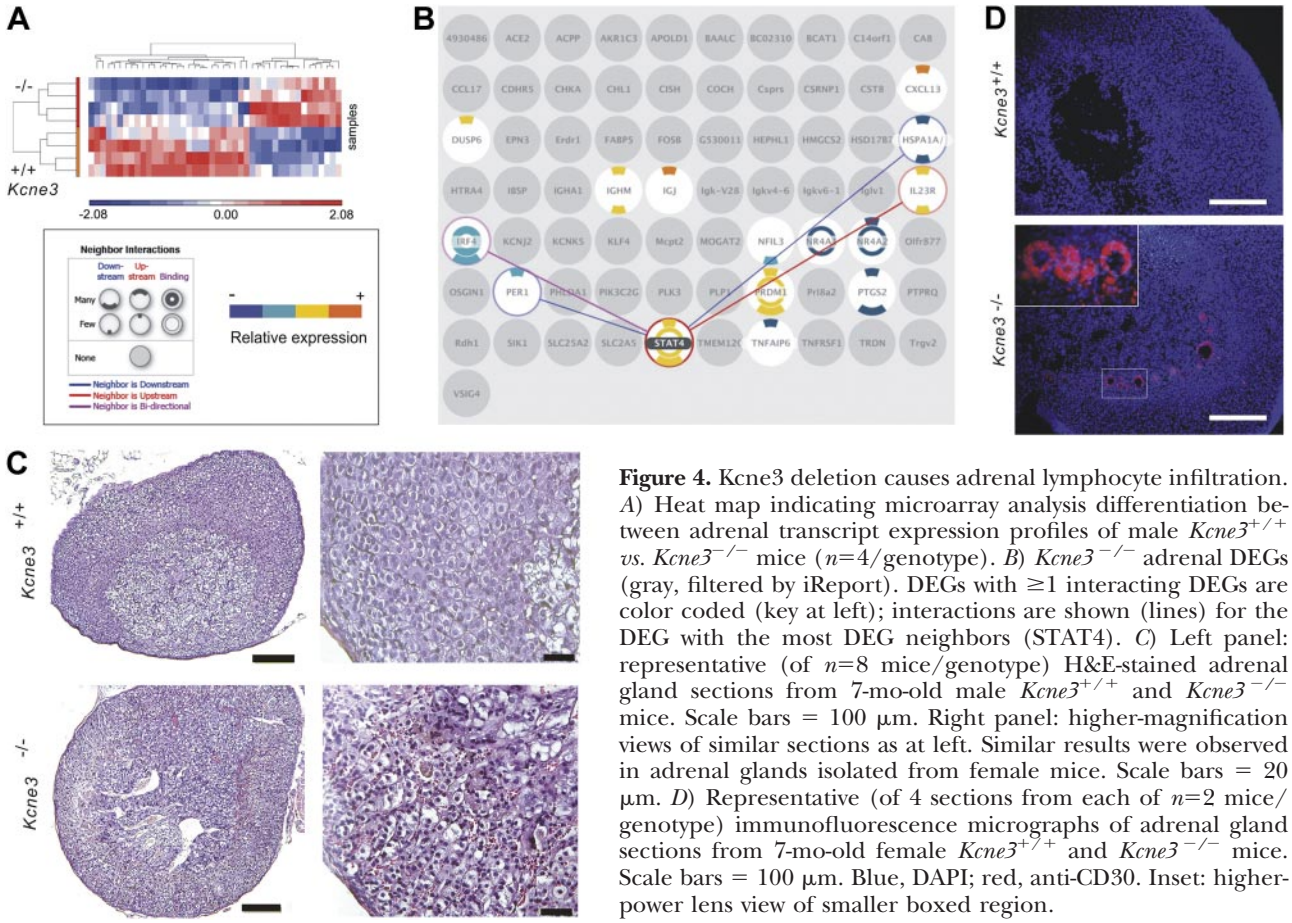

Figure 4. Kcne3 deletion causes adrenal lymphocyte infiltration. *A*) Heat map indicating microarray analysis differentiation between adrenal transcript expression profiles of male $Kcne3^{+/+}$ *vs.* $Kcne3^{-/-}$ mice (n=4/genotype). *B*) $Kcne3^{-/-}$ adrenal DEGs (gray, filtered by iReport). DEGs with ≥1 interacting DEGs are color coded (key at left); interactions are shown (lines) for the DEG with the most DEG neighbors (STAT4). *C*) Left panel: representative (of n=8 mice/genotype) H&E-stained adrenal gland sections from 7-mo-old male $Kcne3^{+/+}$ and $Kcne3^{-/-}$ mice. Scale bars = 100 μm. Right panel: higher-magnification views of similar sections as at left. Similar results were observed in adrenal glands isolated from female mice. Scale bars = 20 μm. *D*) Representative (of 4 sections from each of n=2 mice/genotype) immunofluorescence micrographs of adrenal gland sections from 7-mo-old female $Kcne3^{+/+}$ and $Kcne3^{-/-}$ mice. Scale bars = 100 μm. Blue, DAPI; red, anti-CD30. Inset: higher-power lens view of smaller boxed region.

trate the lower predisposition to reperfusion VT of $Kcne3^{+/+}$ mice compared to $Kcne3^{-/-}$ mice (Fig. 6*A*). In the 2 $Kcne3^{+/+}$ mice exhibiting VT, sinus rhythm was punctuated by brief periods of VT, returning to sinus rhythm within 10 s. In contrast, in $Kcne3^{-/-}$ mice, VT was markedly prolonged, the longest episode lasting 132 s (Fig. 6*C*). Notably, spironolactone pretreatment greatly diminished genotype-dependent differences in reperfusion arrhythmia incidence. Thus while untreated $Kcne3^{-/-}$ mice experienced a higher incidence of arrhythmias than did untreated $Kcne3^{+/+}$ mice (P=0.03; Fig. 6*B*), spironolactone pretreatment successfully reduced this increase in arrhythmia incidence such that there was no genotype-dependent difference in arrhythmia incidence in the spironolactone-pretreated mice (P=0.3; Fig. 6*B*). Spironolactone pretreatment also halved mean reperfusion VT duration in $Kcne3^{-/-}$ mice, from 37.3 ± 14.5 (untreated) to 16.5 ± 13.3 s (spironolactone-pretreated) (Fig. 6*C*) and reduced the incidence in $Kcne3^{-/-}$ mice of sustained VT (>30 s duration) from 45.5 to 10% (P<0.05) without affecting this parameter in the $Kcne3^{+/+}$ mice (Fig. 6*D*).

DISCUSSION

Our findings support a novel mechanism in which *Kcne3* deletion leads to secondary hyperaldosteronism associated with an adrenal-specific lymphocyte infiltration. The increase in serum aldosterone, in turn, causes aldosterone-dependent QT prolongation and predisposes to postischemic reperfusion VT. As we and others (9) could not detect *Kcne3* in mouse heart, the data show for the first time that a monogenic channelopathy can cause arrhythmogenesis in the absence of any primary disruption of cardiac function. In a model also incorporating the hyperlipidemia we observed in $Kcne3^{-/-}$ mice, we contrast the disease etiology suggested by our findings in the $Kcne3^{-/-}$ mice, with the established mechanistic framework for monogenic, channelopathic ventricular arrhythmias (Fig. 6*E*).

Of the 25 human genes associated with or linked to life-threatening ventricular arrhythmias (2), most are not exclusively expressed in the heart. Despite this, the search for mechanistic bases of inherited arrhythmias has been almost exclusively focused on disruption of the cardiac roles of these gene products, a logical place to start. More recently, interest in mechanisms of sudden unexplained death in epilepsy (SUDEP) has brought to the fore the idea that arrhythmia-linked ion channel genes may also be expressed in regions of the brain controlling cardiac function and that seizures caused by their disruption may precipitate or contribute to provoking ventricular arrhythmias. In a recent study, a human LQTS mutant KCNQ1 knocked into mouse brain was found to cause seizures, a potential trigger for cardiac arrhythmias and molecular genetic basis for SUDEP (17). In addition, prior work showed

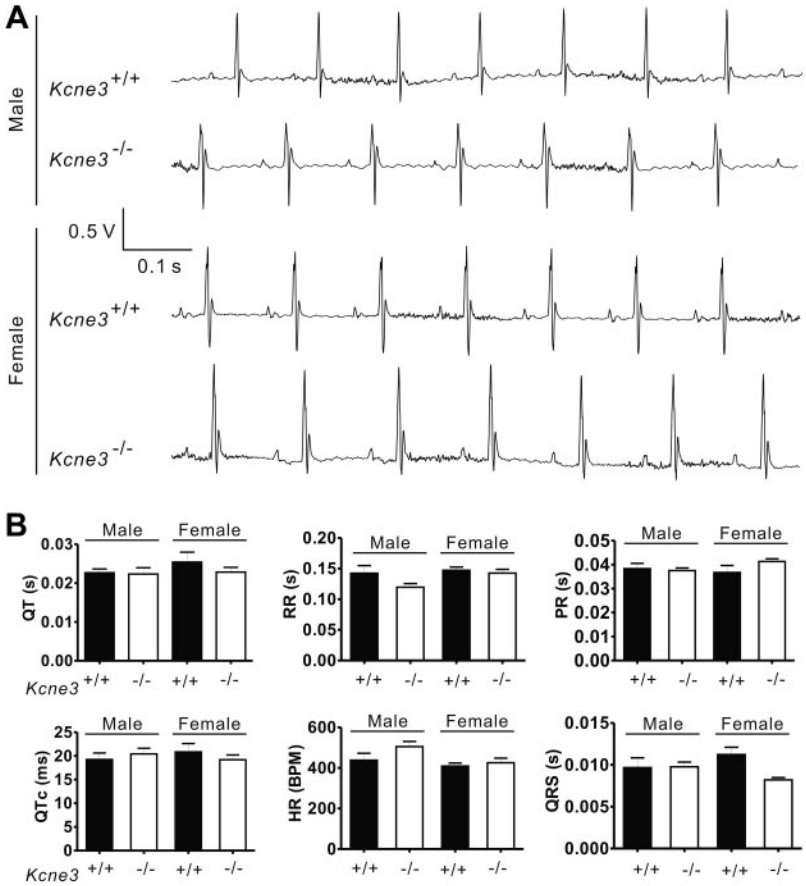

Figure 5. Aldosterone receptor antagonism eliminates QT prolongation arising from *Kcne3* deletion. *A*) Representative (of n=9–10 mice) baseline ECGs recorded from 9-mo-old $Kcne3^{+/+}$ and $Kcne3^{-/-}$ mice pretreated with spironolactone. *B*) Mean ECG parameters of 9-mo-old $Kcne3^{+/+}$ (n=9) and $Kcne3^{-/-}$ (n=10) mice pretreated with spironolactone.

that deletion of *Kcne1*, which is reportedly expressed in the adrenal gland, caused hypokalemia and hyperaldosteronism in mice, but a role for these extracardiac effects in arrhythmogenesis in $Kcne1^{-/-}$ mice was not determined (18).

In the present study, we demonstrate that disruption of a gene that is undetectable in the ventricular or atrial tissue of the $Kcne3^{+/+}$ genotype of the mouse strain we investigated can predispose to ventricular arrhythmogenesis in the absence of detectable structural heart disease. The underlying premise, that hyperaldosteronism can prolong the QT interval (*i.e.,* delay ventricular repolarization) and increase postischemic reperfusion arrhythmia susceptibility, is not novel and indeed is an established mechanism in human arrhythmias (15, 16). Similarly, cardiac-specific overexpression of the mineralocorticoid receptor delays ventricular repolarization in mice (19). Thus, our data are consistent with previous human and mouse studies, as we find that competitive antagonism of the aldosterone receptor with spironolactone eliminates the baseline QT prolongation we observe in older *Kcne3* null mice (statistically significant in females) and diminishes the genotype-dependent predisposition to reperfusion arrhythmias in *Kcne3*-null mice.

Rather, the surprising elements of our study comprise the following 2 findings: first, despite its lack of cardiac expression, *Kcne3* deletion prolongs the QT interval in mice; second, the apparent underlying mechanism of the QT-prolonging hyperaldosteronism. When first investigating the source of hyperaldosteronism in *Kcne3*-null mice, untargeted microarray analysis pointed strongly to an autoimmune-type infiltration, a hypothesis strongly supported by the widespread adrenal infiltration of immune cells, and $CD30^{+}$ cell subpopulation, visible in $Kcne3^{-/-}$ but not $Kcne3^{+/+}$ adrenal sections.

What is not yet formally established is whether the lymphocyte infiltration causes the secondary hyperaldosteronism (secondary because we could not detect *Kcne3* in mouse adrenals) or is a reaction to it. The adrenal microarray evidence (Supplemental Figs. S2 and S3 and Fig. 4) suggests a targeted autoimmune reaction to the adrenal gland in response to increased local expression of C-X-C motif chemokine 13 (CXCL13), a well-established B-cell chemoattractant (11). The disproportionate representation of immunoglobulin κ locus transcript expression increase in the *Kcne3*-null adrenal tissue RNA (reflecting adrenal infiltration of B cells) without the expected, matching increase in immunoglobulin λ locus transcript expression (Supplemental Fig. S2) is consistent with increased abundance of a small clonal population of B cells. This is observed in neoplastic conditions akin to B-cell lymphoma, but is also not uncommon in autoimmune disorders, occurring, for example, in 40% of patients with rheumatoid arthritis in one study (20). The other outstanding question remaining is why *Kcne3* deletion causes the adrenal infiltration: which tissue is defective? KCNE3 is expressed in various blood cell lineages,

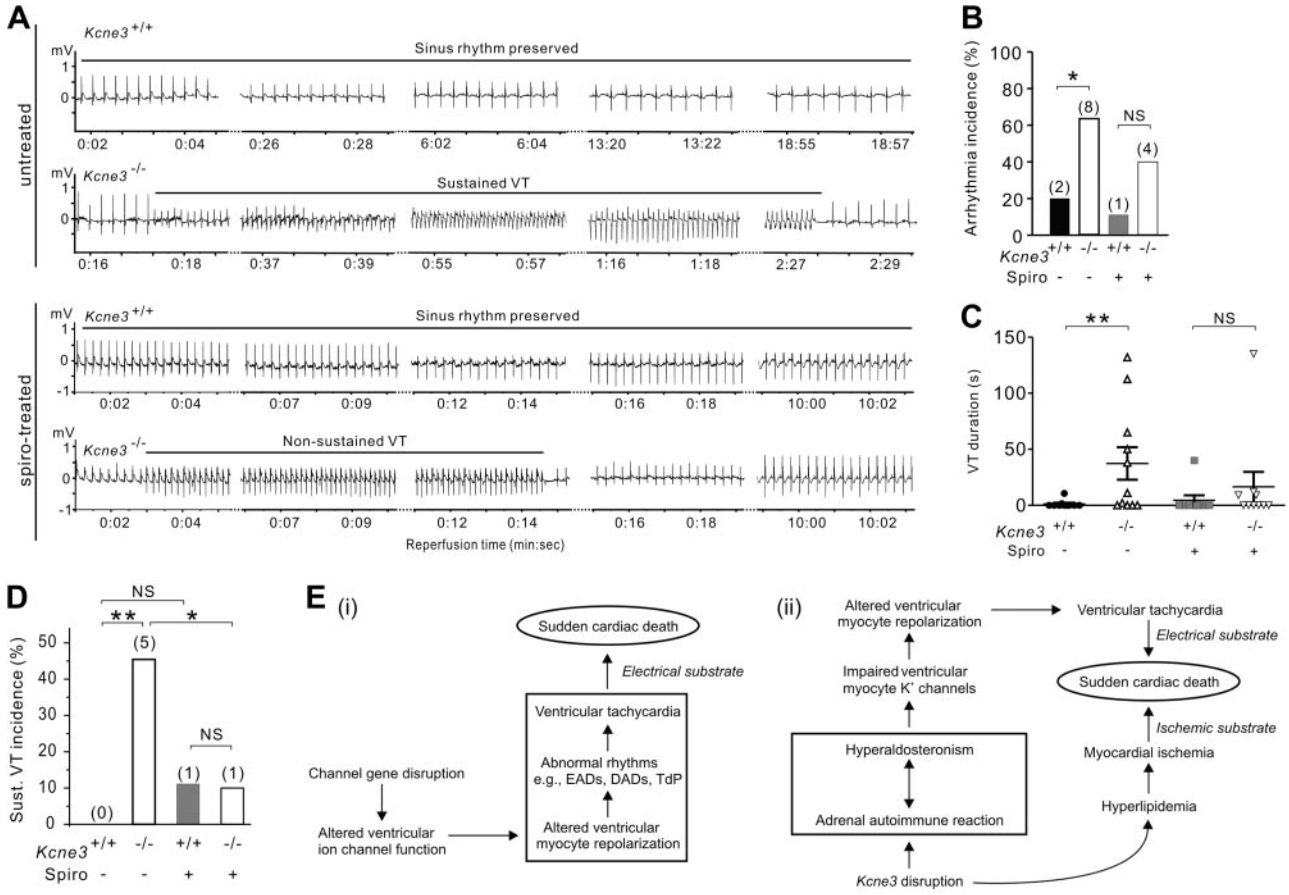

Figure 6. Kcne3 deletion causes an aldosterone-dependent predisposition to postischemia reperfusion VT. *A*) Representative (of n=9–10 mice) ECG traces recorded during reperfusion in untreated or spironolactone (spiro)-pretreated 9-mo-old *Kcne3*$^{+/+}$ and *Kcne3*$^{-/-}$ mice. *B*) Arrhythmia incidence during postischemia reperfusion in 9-mo-old mice with (n=9–10) or without (n=10–11) spironolactone pretreatment. Values in parentheses indicate number of mice exhibiting arrhythmia per group. N.S., not significant (P=0.3 between genotypes). *$P < 0.05$ between genotypes. *C*) VT duration (individual indicated by symbols; mean indicated by horizontal line) for mice as in *B* (mice not exhibiting VT included and indicated as 0 duration). **$P < 0.01$ between genotypes. *D*) Sustained (>30 s) VT incidence during postischemia reperfusion in 9-mo-old mice with (n=9–10) or without (n=10–11) spironolactone pretreatment. Values in parentheses indicate number of mice exhibiting sustained VT per group. N.S. = $P > 0.05$ between genotypes. *$P < 0.05$. **$P < 0.01$ between genotypes. *E*) *i*) Existing model for the mechanism of monogenic channelopathic predisposition to SCD. *ii*) Multifactorial etiology of *Kcne3*-associated arrhythmogenesis and SCD suggested for the *Kcne3*$^{-/-}$ mouse model, supported by the findings herein. DADs, delayed afterdepolarizations; EADs, early afterdepolarizations; TdP, torsades de pointe.

but its role in these cells is not known (21) and certainly also warrants further investigation.

Finally, what can these findings teach us about the role of KCNE3 in human ventricular arrhythmias? KCNE3 mutations (T4A and R99H) have been found in patients with BrS, the latter in 4/4 phenotype-positive family members *vs.* 0/3 phenotype-negative. In both cases, heterologous examination of the KCNE3 mutants revealed that they increased currents through channels formed with KCNE3 and $K_V4.3$ (KCND3) compared to wild-type complexes (22, 23). Furthermore, KCNE3 protein expression was reported in adult human atrial appendage and rat ventricular tissue, as were $K_V4.3$-KCNE3 protein complexes (22). These findings suggest a direct cardiac role for KCNE3 in human and rat, with the caveat that in the absence of robust negative controls (such as knockout tissue) it is challenging to reliably verify expression of small, transmembrane proteins in cardiac tissue. Increased ventricular I_{to} would certainly make sense for a mechanism contributing to BrS, which is most commonly associated with loss-of-function mutations in the SCN5A cardiac voltage-gated sodium channel gene. The T4A and R99H KCNE3 variants were also isolated from individuals who experienced drug- or hypokalemia-triggered torsades de pointe, and in heterologous expression studies found to reduce current density through KCNQ1-KCNE3 channels (22, 24). Again, this mechanism is consistent with accepted models of inherited loss of repolarization reserve predisposing to ventricular arrhythmogenesis when an additional challenge (drug or hypokalemia) is imposed (25).

While the mouse would appear to be different with respect to the lack of cardiac *Kcne3* expression, this does not rule out additional extracardiac manifestations of human *KCNE3* mutants that could contribute to ventricular arrhythmogenesis. This will be difficult to evaluate because of the relative rarity of identified

human *KCNE3*-associated ventricular arrhythmias, but could be feasible for the more commonly arrhythmia-linked KCNQ1 gene, widely expressed in secretory epithelia and regulated by KCNE3 in intestinal and airway epithelial cells (9).

In addition to elucidating the mechanistic basis for adrenal lymphocyte infiltration, future investigations will examine the cause of hyperlipidemia in *Kcne3*-null mice (Fig. 3*C*), and whether this contributes to modulating the functional properties of ventricular K^+ channels by altering ventricular myocyte membrane composition (26). Studies into the specific molecular mechanistic basis for aldosterone-dependent proarrhythmia in $Kcne3^{-/-}$ mice are also needed to explain why QT_c is lengthened despite slowed $I_{K,slow1}$ inactivation in isolated myocytes. This could involve, *e.g.*, aldosterone-dependent augmentation of calcium current and decrease in I_{to} (ref. 27; a trend for which was observed here in $Kcne3^{-/-}$ mice). FJ

The authors thank Dr. Vikram Kanda for expert technical assistance. The authors are grateful for financial support from the U.S. National Institutes of Health—National Heart, Lung and Blood Institute (HL079275 to G.W.A.; HL034215 to R.L.) and University of California–Irvine setup funds (to G.W.A.).

REFERENCES

1. Napolitano, C. (2012) Genetic testing of inherited arrhythmias. *Pediatr. Cardiol.* **33,** 980–987
2. George, A. L., Jr. (2013) Molecular and genetic basis of sudden cardiac death. *J. Clin. Invest.* **123,** 75–83
3. McCrossan, Z. A., and Abbott, G. W. (2004) The MinK-related peptides. *Neuropharmacology* **47,** 787–821
4. Roepke, T. K., King, E. C., Purtell, K., Kanda, V. A., Lerner, D. J., and Abbott, G. W. (2011) Genetic dissection reveals unexpected influence of beta subunits on KCNQ1 K+ channel polarized trafficking *in vivo*. *FASEB J.* **25,** 727–736
5. Mitchell, G. F., Jeron, A., and Koren, G. (1998) Measurement of heart rate and Q-T interval in the conscious mouse. *Am. J. Physiol.* **274,** H747–751
6. Roepke, T. K., Kontogeorgis, A., Ovanez, C., Xu, X., Young, J. B., Purtell, K., Goldstein, P. A., Christini, D. J., Peters, N. S., Akar, F. G., Gutstein, D. E., Lerner, D. J., and Abbott, G. W. (2008) Targeted deletion of kcne2 impairs ventricular repolarization via disruption of I(K,slow1) and I(to,f). *FASEB J.* **22,** 3648–3660
7. Koyama, M., Seyedi, N., Fung-Leung, W. P., Lovenberg, T. W., and Levi, R. (2003) Norepinephrine release from the ischemic heart is greatly enhanced in mice lacking histamine H3 receptors. *Mol. Pharmacol.* **63,** 378–382
8. Abbott, G. W. (2013) KCNE genetics and pharmacogenomics in cardiac arrhythmias: much ado about nothing? *Expert Rev. Clin. Pharmacol.* **6,** 49–60
9. Preston, P., Wartosch, L., Gunzel, D., Fromm, M., Kongsuphol, P., Ousingsawat, J., Kunzelmann, K., Barhanin, J., Warth, R., and Jentsch, T. J. (2010) Disruption of the K+ channel beta-subunit KCNE3 reveals an important role in intestinal and tracheal Cl- transport. *J. Biol. Chem.* **285,** 7165–7175
10. Mackins, C. J., Kano, S., Seyedi, N., Schafer, U., Reid, A. C., Machida, T., Silver, R. B., and Levi, R. (2006) Cardiac mast cell-derived renin promotes local angiotensin formation, norepinephrine release, and arrhythmias in ischemia/reperfusion. *J. Clin. Invest.* **116,** 1063–1070
11. Gunn, M. D., Ngo, V. N., Ansel, K. M., Ekland, E. H., Cyster, J. G., and Williams, L. T. (1998) A B-cell-homing chemokine made in lymphoid follicles activates Burkitt's lymphoma receptor-1. *Nature* **391,** 799–803
12. Parham, C., Chirica, M., Timans, J., Vaisberg, E., Travis, M., Cheung, J., Pflanz, S., Zhang, R., Singh, K. P., Vega, F., To, W., Wagner, J., O'Farrell, A. M., McClanahan, T., Zurawski, S., Hannum, C., Gorman, D., Rennick, D. M., Kastelein, R. A., de Waal Malefyt, R., and Moore, K. W. (2002) A receptor for the heterodimeric cytokine IL-23 is composed of IL-12Rbeta1 and a novel cytokine receptor subunit, IL-23R. *J. Immunol.* **168,** 5699–5708
13. Belladonna, M. L., Renauld, J. C., Bianchi, R., Vacca, C., Fallarino, F., Orabona, C., Fioretti, M. C., Grohmann, U., and Puccetti, P. (2002) IL-23 and IL-12 have overlapping, but distinct, effects on murine dendritic cells. *J. Immunol.* **168,** 5448–5454
14. Kaudewitz, P., Stein, H., Burg, G., Mason, D. Y., and Braun-Falco, O. (1986) Atypical cells in lymphomatoid papulosis express the Hodgkin cell-associated antigen Ki-1. *J. Invest. Dermatol.* **86,** 350–354
15. Gao, X., Peng, L., Adhikari, C. M., Lin, J., and Zuo, Z. (2007) Spironolactone reduced arrhythmia and maintained magnesium homeostasis in patients with congestive heart failure. *J. Cardiac Failure* **13,** 170–177
16. Wei, J., Ni, J., Huang, D., Chen, M., Yan, S., and Peng, Y. (2010) The effect of aldosterone antagonists for ventricular arrhythmia: a meta-analysis. *Clin. Cardiol.* **33,** 572–577
17. Goldman, A. M., Glasscock, E., Yoo, J., Chen, T. T., Klassen, T. L., and Noebels, J. L. (2009) Arrhythmia in heart and brain: KCNQ1 mutations link epilepsy and sudden unexplained death. *Sci. Transl. Med.* **1,** 2ra6
18. Arrighi, I., Bloch-Faure, M., Grahammer, F., Bleich, M., Warth, R., Mengual, R., Drici, M. D., Barhanin, J., and Meneton, P. (2001) Altered potassium balance and aldosterone secretion in a mouse model of human congenital long QT syndrome. *Proc. Natl. Acad. Sci. U. S. A.* **98,** 8792–8797
19. Ouvrard-Pascaud, A., Sainte-Marie, Y., Benitah, J. P., Perrier, R., Soukaseum, C., Nguyen Dinh Cat, A., Royer, A., Le Quang, K., Charpentier, F., Demolombe, S., Mechta-Grigoriou, F., Beggah, A. T., Maison-Blanche, P., Oblin, M. E., Delcayre, C., Fishman, G. I., Farman, N., Escoubet, B., and Jaisser, F. (2005) Conditional mineralocorticoid receptor expression in the heart leads to life-threatening arrhythmias. *Circulation* **111,** 3025–3033
20. McGee, B., Small, R. E., Singh, R., Han, J., Carlson, P. L., Ruddy, S., and Moxley, G. (1996) B lymphocytic clonal expansion in rheumatoid arthritis. *J. Rheumatol.* **23,** 36–43
21. Sole, L., Vallejo-Gracia, A., Roig, S. R., Serrano-Albarras, A., Marruecos, L., Manils, J., Gomez, D., Soler, C., and Felipe, A. (2013) KCNE gene expression is dependent on the proliferation and mode of activation of leukocytes. *Channels (Austin)* **7,** 85–96
22. Delpon, E., Cordeiro, J. M., Nunez, L., Thomsen, P. E., Guerchicoff, A., Pollevick, G. D., Wu, Y., Kanters, J. K., Larsen, C. T., Hofman-Bang, J., Burashnikov, E., Christiansen, M., and Antzelevitch, C. (2008) Functional effects of KCNE3 mutation and its role in the development of Brugada syndrome. *Circ. Arrhythmia Electrophysiol.* **1,** 209–218
23. Nakajima, T., Wu, J., Kaneko, Y., Ashihara, T., Ohno, S., Irie, T., Ding, W. G., Matsuura, H., Kurabayashi, M., and Horie, M. (2012) KCNE3 T4A as the genetic basis of Brugada-pattern electrocardiogram. *Circ. J.* **76,** 2763–2772
24. Ohno, S., Toyoda, F., Zankov, D. P., Yoshida, H., Makiyama, T., Tsuji, K., Honda, T., Obayashi, K., Ueyama, H., Shimizu, W., Miyamoto, Y., Kamakura, S., Matsuura, H., Kita, T., and Horie, M. (2009) Novel KCNE3 mutation reduces repolarizing potassium current and associated with long QT syndrome. *Human Mutation* **30,** 557–563
25. Roden, D. M. (1996) Ionic mechanisms for prolongation of refractoriness and their proarrhythmic and antiarrhythmic correlates. *Am. J. Cardiol.* **78,** 12–16
26. Abi-Char, J., Maguy, A., Coulombe, A., Balse, E., Ratajczak, P., Samuel, J. L., Nattel, S., and Hatem, S. N. (2007) Membrane cholesterol modulates Kv1.5 potassium channel distribution and function in rat cardiomyocytes. *J. Physiol.* **582,** 1205–1217
27. Benitah, J. P., Perrier, E., Gomez, A. M., and Vassort, G. (2001) Effects of aldosterone on transient outward K+ current density in rat ventricular myocytes. *J. Physiol.* **537,** 151–160

Received for publication August 28, 2013.
Accepted for publication November 4, 2013.